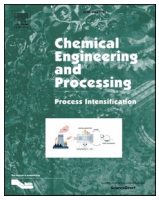
Chemical Engineering & Processing: Process Intensification 216 (2025) 110428



Contents lists available at ScienceDirect

Chemical Engineering and Processing - Process Intensification

journal homepage: www.elsevier.com/locate/cep





Cyclic aqueous carbonation of fly ash in seawater: Enhancing carbonation efficiency and CO_2 removal rate

Tianle Cheng [a,b], Zesheng Ding [a], Xu Zhang [a], Jiajun Chai [a], Yunwen Shen [a], Lihong Cai [c], Rui Bao [d], Ying Chen [a], Yiwen Pan [a,b,*]

[a] State Key Laboratory of Ocean Sensing & Ocean College, Zhejiang University, Zhoushan 316021, China
[b] Hainan Engineering Research Center for Marine Environmental Monitoring and Detection Equipment, Hainan Institute of Zhejiang University, Sanya 572025, China
[c] Yuanchu Tech. Beijing Co. Ltd, Beijing 100101, China
[d] Frontiers Science Center for Deep Ocean Multispheres & Earth, Key Laboratory of Marine Chemistry Theory & Technology, Ministry of Education, Ocean University of China, Qingdao 266100, China

ARTICLE INFO

Keywords:
CO_2 mineralization
Process intensification
Aqueous carbonation
Seawater
Coal fly ash
pCO_2

ABSTRACT

Aqueous mineral carbonation of coal fly ash (CFA) is an effective CO_2 sequestration strategy, but improving its efficiency remains challenging. We observed a significant drop in carbonation efficiency from 94.8 % to 26.5 % when transitioning from an open to a sealed system using the same CaO-content CFA and seawater under ambient conditions. Experiments revealed that the slightly elevated pCO_2 in the sealed system accelerated $CaCO_3$ formation on CFA surfaces, hindering CaO leaching. To address this, we proposed introducing excess CO_2 post-carbonation to dissolve external $CaCO_3$, facilitating further CaO leaching and enhancing efficiency through a cyclic carbonation method. After optimizing the process with this cyclic approach, under identical conditions, the carbonation efficiency increased from 26.5 % (cycle 1) to 31.3 % (cycle 3) and CO_2 removal rate from 65.6 % to 80.3 %. Optimized solid-to-liquid and magnesium-to-calcium ratios during the cycles further improved efficiency. These findings provide valuable insights for enhancing industrial carbonation and CO_2 capture.

1. Introduction

Climate change challenges underscore the inadequacy of natural CO_2 absorption by land and oceans, which averaged 6.0 ± 1.0 GtC annually from 2012 to 2021, compared to 11.2 GtC of anthropogenic emissions from fossil fuels and land-use changes in 2023 [1]. Achieving net-zero CO_2 emissions clearly requires human intervention. Historical data from 1850 to 2022 show that 69 % of emissions came from fossil fuels, with coal combustion accounting for 46 % [1,2]. Under China's "Dual Carbon" strategy, reducing CO_2 emissions from coal-fired power plants is crucial for achieving strategic goals [3–6]. Post-combustion CO_2 capture (PCC) is a promising approach to rapidly reduce greenhouse gas emissions from coal-fired and other fossil fuel power plants [7]. The mineral carbonation (MC), also known as mineral sequestration, proposed by Olajire, offers a scheme for permanently sequestering CO_2 without leakage [8]. Generally, mineral carbonation can be carried out using alkaline-rich natural rocks, or industrial solid wastes or by-products with high Ca or Mg content, such as fly ash [9–11], steel slag [12–14], cement kiln dust [15,16], and waste cement [17,18], among others.

Coal fly ash (CFA), a complex and non-uniform by-product of coal combustion in coal-fired power stations, reached a production of 580 Mt in China in 2015 [19–22]. Characterized by its relatively high reactivity and inherent alkalinity, coupled with its immediate availability in the vicinity of industrial facilities, CFA serves as an exemplary substrate for mineral carbonation [23–28]. The resultant carbonated products from CFA, when utilized as supplementary cementitious materials in cementitious matrices and concrete blocks, contribute to an indirect reduction in CO_2 emissions [29].The content of free calcium oxide (f-CaO) in raw CFA is a critical parameter for its application as an auxiliary gelling material in cement, with the European regulatory framework setting a maximum allowable limit of 1.5 wt. % for f-CaO in cement additives [30]. Exceeding this threshold may precipitate durability concerns in cementitious materials. The process of carbonation presents a solution to the issue of elevated f-CaO levels in CFA. Wei et al. has demonstrated that the carbonation of CFA can augment the strength of cement-CFA blends, with the enhancement in strength being directly proportional to the extent of carbonation (CO_2 uptake) [31]. This discovery provides an expanded range of applications for carbonated CFA.

* Corresponding author at: State Key Laboratory of Ocean Sensing & Ocean College, Zhejiang University, Zhoushan, 316021, China.
E-mail address: evelynpan@zju.edu.cn (Y. Pan).

https://doi.org/10.1016/j.cep.2025.110428
Received 8 March 2025; Received in revised form 9 June 2025; Accepted 29 June 2025
Available online 2 July 2025
0255-2701/© 2025 Elsevier B.V. All rights are reserved, including those for text and data mining, AI training, and similar technologies.

In the field of CFA mineral carbonation, carbonation efficiency under ambient conditions is typically below 31 % and varied with the type of CFA [32–35]. In our previous study, we achieved an extremely high carbonation efficiency of 94.8 % using CFA containing 8.04 wt. % CaO in an open beaker at ambient temperature and pressure [11]. To explore industrial application, we sealed the process while keeping other conditions unchanged. However, the carbonation efficiency dropped significantly to levels comparable to those reported by Jo et al. [32]. This suggests that the efficiency reduction is likely due to elevated pCO_2 in the sealed system, rather than the type of CFA, although different CFA types can indeed affect carbonation efficiency [35]. Sealed systems, essential for industrial applications to prevent dust escape and enable exhaust gas recycling [36], can elevate pCO_2 levels, accelerating $CaCO_3$ formation in the solution and at the solid-liquid interface [37,38]. Rapid $CaCO_3$ formation at the interface hinders CaO leaching, reducing utilization efficiency [39,40]. This shows that, in addition to pH and Mg/Ca, pCO_2 significantly impacts carbonation efficiency.

In this study, we demonstrated how pCO_2 affects carbonation efficiency and explore the underlying mechanisms. Based on these insights, we developed a universal cyclic carbonation process using 8.04 wt. % CaO CFA and artificial seawater under ambient temperature and sealed conditions. By introducing excess CO_2 into the solution after $CaCO_3$ has fully precipitated, $CaCO_3$ would be dissolve, which in turn promoted further leaching of CaO and enhanced the carbonation efficiency.

The carbonate parameters in both the solution and solid precipitates were systematically analyzed. The carbonation efficiency of CFA and CO_2 removal rate were determined using thermogravimetric analysis (TGA) and direct flow rate monitoring, respectively. Further clarification of the mechanisms for improving efficiency was achieved through comparative experiments by varying the solid-to-liquid ratio (S/L) and magnesium-to-calcium ratio (Mg/Ca). Finally, the feasibility of this method for industrial application was analyzed from a cost perspective, providing a new solution for carbon emission reduction in coastal coal-fired power plants.

2. Materials and methods

2.1. Materials

The raw CFA, sourced from Zhejiang Petrochemical & Co., Ltd., was used without sieving. Its composition was analyzed using X-ray Diffraction (XRD) and X-ray Fluorescence Spectrometry (XRF, Epsilon 1, PANalytical, Netherlands). The CFA primarily consisted of SiO_2 (45.57 wt. %), Al_2O_3 (39.98 wt. %), CaO (8.04 wt. %), Fe_2O_3 (3.06 wt. %), and MgO (0.19 wt. %). The artificial seawater used in the experiments was prepared according to the ASTM D1141–98 standard practice for the preparation of substitute ocean water.

2.2. Experiment procedure

For industrial applications, we employ a sealed system and propose an innovative cyclic seawater carbonation method to enhance its carbonation efficiency. By facilitating the dissolution of $CaCO_3$ and leaching more CaO from CFA, excess CO_2 was introduced into the solution until the pH dropped to approximately 6.5 before starting the next cycle.

This experiment conducted three cycles using the cyclic seawater carbonation method:

Cycle 1: At 25 ℃, 40 g of CFA was added to 600 mL of artificial seawater in a sealed container, resulting in an initial S/L of 68 g/L.The mixture was stirred at 800 rpm for 1 h to ensure complete dispersion and Ca leaching. High-purity CO_2 (99.99 %) was then introduced at 40 mL/min, causing the pH to drop. Solid samples were taken for TGA when the pH reached 8.2, indicating maximum $CaCO_3$ precipitation [11]. The cycle ended when the pH fell below 6.5.

Cycle 2: After Cycle 1, another 80 g of raw CFA was added under the same conditions. This addition increased the S/L to 204 g/L. After 1 h of stirring, CO_2 was introduced at 40 mL/min. Solid samples were taken for TGA at pH 8.2, and the cycle ended when the pH dropped below 6.5.

Cycle 3: After Cycle 2, a further 80 g of raw CFA was added under the same conditions, elevating the S/L to 340 g/L. After 1 h of stirring, CO_2 was introduced at 40 mL/min. Solid samples were taken for TGA at pH 8.2, and the cycle ended at this point (to avoid excessive pCO_2 becoming a carbon source at pH 6.5, with minimal pCO_2 and near-seawater pH at endpoint)

The core principle of fixedly adding 80 g CFA in cycles 2–3: This quantity is selected to rapidly fix the excess CO_2 in the slurry from the previous cycle and raise the pH above 10.0, thereby ensuring feasible carbonation conditions.

During the experimental process, an electronic flowmeter was utilized to monitor the gas outlet velocity. Additionally, a pH sensor array developed in our previous research [41,42] was employed to monitor the pH of the solution, collecting pH data. The data were calibrated against three NIST traceable buffer solutions (4.01, 7.00, and 10.01) at 25 ℃ using a commercial pH sensor (Orion Ross, Thermo Fisher, USA).

In the experiment, a sampling syringe (pre-rinsed with DI water) was used to withdraw a liquid volume of 10 mL each time, and the liquid samples were immediately filtered through a PES filter membrane with a pore size of 0.45 μm. Both liquid and solid samples were withdrawn for analysis. The dissolved inorganic carbon (DIC) in the solution was measured using a DIC analyzer (AS-C5, Apollo, USA) [Ca^{2+}] and [Mg^{2+}] were also determined by high-precision ion chromatography (ICS-5000+, Thermo Fisher, USA), using IAPSO seawater (batch P166) as a reference. The precision of DIC, [Ca^{2+}], and [Mg^{2+}] measurements was all higher than 0.1 %. Additionally, we use the CO2SYS program developed by Lewis and Wallace to convert DIC and pH pairs to the pCO_2 [43]. The solid samples' weight loss curves during heating were measured by a thermogravimetric analyzer (TGA/DSC3+), which allowed for the calculation of the mass of $CaCO_3$ generated during the carbonation process. The thermogravimetric analyzer was set with an initial temperature of 50 ℃ and heated to 950 ℃ at a rate of 10 ℃/min in a nitrogen atmosphere.

To explore the mechanism by which the cyclic seawater carbonation method of CFA enhances carbonation efficiency, we designed comparative experiments. Different masses of CFA were added to seawater to obtain slurries with specific S/L (17, 34, 68 and 136 g/L). High-purity CO_2 gas (99.99 %) was introduced into a sealed container and bubbled through the slurry at a gas flow rate of 40 mL/min. The experimental results were compared with data from identical S/L in the previous study conducted under an open system to investigate the influence of different systems on reaction efficiency [11]. Experiments with varying Mg/Ca were conducted by adding different masses of $MgCl_2{\cdot}6H_2O$ and CaO to magnesium-free artificial seawater to achieve specific Mg/Ca (0, 5, and 7.5). High-purity CO_2 gas (99.99 %) was introduced at 40 mL/min into the sealed container, bubbling through the solution to study the impact of Mg/Ca on the carbonation efficiency.

Fig. 1 shows schematics of open and sealed systems. In prior open-system experiments, the reactor was fully open without outlet gas monitoring; reaction completion was determined solely by pH measurement. In this study's sealed-system experiments, the reactor remained sealed (gas ports sealed; system sealed after CFA addition until reaction completion). Reaction completion was similarly confirmed by pH measurement, with electronic outlet flowmeters added to monitor gas flow rate changes.

2.3. Calculation of sequestration capacity, carbonation efficiency and CO_2 removal rate

In industrial applications, the current assessment of the carbonation capacity of CFA has limitations. Existing evaluation indicators mostly focus on carbonation efficiency and the amount of CO_2 in solid CFA. However, in the industrial field, the key is how to effectively remove

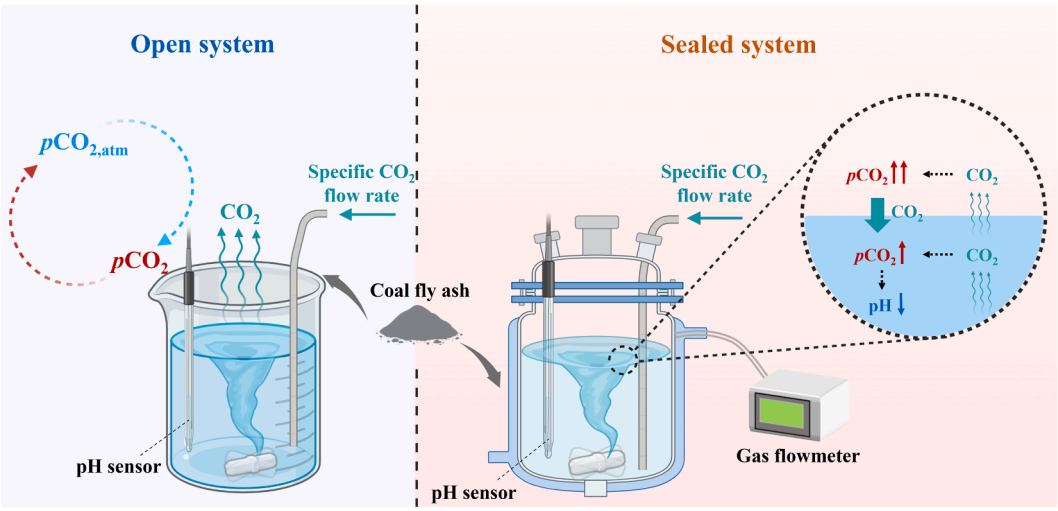


Fig. 1. Schematic of open (left) and sealed (right) systems.

CO_2 from waste gas to achieve emission reduction, which is closely related to the overall CO_2 removal rate of the system. Therefore, attention should not be limited to the fixation of CO_2 by solid CFA. The CO_2 removal rate, defined as the ratio of CO_2 sequestered to the total inflow, provides a more accurate measure of the overall carbonation efficiency in the CFA aqueous carbonation system and is suitable as an assessment indicator in industrial applications. Therefore, this study advocates incorporating the CO_2 removal rate into the evaluation framework to more comprehensively and accurately assess the carbonation capacity of CFA in practical applications.

The carbonation efficiency (ζCa(%)) and CO_2 sequestration capacity ($SeCO_2$) are key parameters for evaluating CFA's carbon sequestration capability. $SeCO_2$ (kg CO_2/ t CFA) refers to the CO_2 sequestration capacity of CFA, indicating the mass of CO_2 that can be immobilized per unit mass of CFA. ζCa(%) signifies the carbonation efficiency of the CFA, reflecting the extent of the carbonation reaction. Both $SeCO_2$ and ζCa(%) can be calculated using XRF (X-ray Fluorescence) and TGA data.

Ji et al. [44] explored the causes of mass loss in CFA at different temperatures through TGA-MS (Thermal Gravimetrical Analysis-Mass Spectrometry) analysis. It was found that the mass loss of CFA within the temperature ranges of 30 ℃ −105 ℃, 105 ℃- 600 ℃, and 600 ℃ - 950 ℃ was attributed to the evaporation of water, thermal decomposition of hydroxides, and thermal decomposition of carbonates, respectively. Therefore, by calculating the mass loss due to the thermal decomposition of carbonates within the 600 ℃ - 950 ℃ range, the mass of $CaCO_3$ generated during the carbonation process can be determined. Subsequently, the mass of CaO involved in the carbonation reaction can be calculated. By combining this with the total calcium content in the original CFA, the carbonation efficiency of the CFA's carbon sequestration can be derived.

CO_2(%), indicating the increase in CO_2 due to carbonation, is calculated using Eq. (1).

$$CO_2(wt\%) = \frac{\Delta w_{600^\circ C-950^\circ C}}{w_{105^\circ C}} - \frac{\Delta w_{600^\circ C-950^\circ C,0}}{w_{105^\circ C,0}} \quad (1)$$

Here, $w_{105\,^\circ C}$ and $w_{105\,^\circ C,0}$ denote the mass fractions of the dry weights of the carbonated and pristine samples, respectively, at 105 °C relative to their initial masses. Additionally, $\Delta w_{600\,^\circ C-950\,^\circ C}$ and $\Delta w_{600\,^\circ C-950\,^\circ C,0}$ represent the differential mass fractions between the carbonated and original samples within the 600 °C - 950 °C temperature range.

The $SeCO_2$, which represents the amount of CO_2 sequestered per t of CFA, can be calculated using Eq. (2).

$$SeCO_2(\text{kg CO2 / t CFA}) = CO_2(wt\%) \times 1000 \quad (2)$$

ζCa(%) is determined by Eq. (3).

$$\zeta Ca(\%) = \frac{CO_2(wt\%)/M_{CO2}}{Ca_{total}(wt\%)/M_{Ca}} \times 100 \quad (3)$$

where

$$Ca_{total}(wt\%) = \frac{\frac{1-CO_2(wt\%)}{1} \times m_{105^\circ C}(g) \times CaO(wt\%) \times \frac{M_{Ca}}{M_{CaO}}}{m_{105^\circ C}(g)} \times 100\%$$

$$= (1 - CO_2(wt\%)) \times CaO(wt\%) \times \frac{M_{Ca}}{M_{CaO}} \times 100 \quad (4)$$

The total calcium content in CFA is determined by Eq. (4). $m_{105\,^\circ C}(g)$ refers to the dry weight of the carbonated sample at 105 °C. The molar masses of CO_2, Ca, and CaO are represented by M_{CO2}, M_{Ca}, and M_{CaO}, with values of 44 g/mol, 40 g/mol, and 56 g/mol, respectively.

$$CO_{2\,removal}(\%) = \frac{m_{absorb}}{m_{total}} \times 100\% = \frac{V_{absorb}}{V_{total}} \times 100\% = \frac{V_{total} - V_{out}}{V_{total}} \times 100\% \quad (5)$$

$CO_{2removal}$, representing the CO_2 removal rate, refers to the percentage of carbon dioxide gas fixed through mineralization reactions relative to the mass of carbon dioxide gas introduced. In this study, experiments were conducted using high-purity CO_2 gas. By disregarding the dissolved gases originally present in seawater, the gas emitted at the outlet is exclusively high-purity CO_2. The difference in flow rates between the inlet and outlet is used to calculate the CO_2 removal rate instead of mass.

The total volume of CO_2 absorbed by the carbon fixation device during the experiment is denoted as V_{absorb}. The total volume of CO_2 gas introduced, V_{total}, is the product of the flow rate Q (mL/ min) and the total gas flow time t_{total} (min). The total volume of gas emitted at the outlet during the gas supply process, V_{out}, is recorded using a micro-nano flowmeter. The flowrates are taken every three seconds, which are defined as the average value of the gas flow at the outlet for that interval. These readings are then multiplied to obtain the total volume of gas emitted at the outlet for each three-second period. Upon completion of the experiment, the cumulative total of these volumes yields V_{out}.

3. Results and discussion

3.1. Differences between open and sealed systems

Fig. 2 shows a comparative analysis of carbonation efficiency between sealed and open systems, with all other parameters held constant. In both open and sealed systems, carbonation efficiency increased with higher S/L. However, this increase was insignificant compared to the dramatic drop in efficiency when transitioning from an open to a sealed system. For example, at an S/L of 68 g/L, carbonation efficiency plummeted from 94.8 % in the open system to 26.5 % in the sealed system, a decrease of nearly 70 %.

By examining the carbonation phases depicted in Fig. 2a and b, we found that the most significant difference between the two systems is the extended duration of the phase with pH > 8.2. At an S/L of 68 g/L, the aeration time in the open system is approximately five times longer than that in the sealed system. Moreover, a closer look at the pH decline during the carbon sequestration phase reveals that the rate and pattern of pH decrease differ markedly. In the open system, the pH decreases much more slowly than in the sealed system, especially in the high S/L group. During the middle and later stages of CO_2 aeration, we observe a slight buffering of pH, likely due to the continuous leaching of CaO. In contrast, in the sealed system, the pH decline is nearly linear with time. This indicates that the duration of the carbonation stage is a critical factor in enhancing carbonation efficiency, and the slightly elevated pCO_2 in the sealed system is likely the key factor shortening the carbonation process.

To further verify the impact of pCO_2 on carbonate sequestration rates, we designed another set of experiments. By reducing the purity of aeration CO_2 in the sealed system, thereby lowering the pCO_2 value, we examined its effect on CO_2 removal rates. Experimental results show that at a gas flow rate of 100 mL/min, the 15 % CO_2 + 85 % N_2 group achieved the highest CO_2 removal rate (97.5 %), significantly outperforming pure CO_2 (53.3 %) and the 75 % CO_2 + 25 % N_2 group (46.3 %). During the carbonation phase, only the 15 % CO_2 group exhibited a slow pH decline, taking 76.1 min to reach pH = 8.2, which is 4.8 times and 3.6 times longer than the pure CO_2 group (15.8 min) and the 75 % CO_2 group (21.8 min), respectively (Fig. 3).

Based on this insight, the high pCO_2 in a sealed system is the primary reason for the difference in carbonation efficiency compared to an open system. In contrast to an open system, the mineralization reaction in a sealed system shortens the carbonation time, accelerates the formation of calcium carbonate on the CFA surface, reduces the leaching rate of CaO, and ultimately leads to a decrease in carbonation efficiency.

3.2. Parameter monitoring in cyclic experiments

The experiments were conducted under ambient temperature in a sealed system with an initial S/L of 68 g/L.Variations in DIC, $[Ca^{2+}]$, $[Mg^{2+}]$ and pCO_2 are illustrated in Fig. 4. Taking Cycle 1 as an example, when excess CO_2 flowing into the system (labeled in yellow), DIC increased significantly from 5382 μM to approximately 28,563 μM $[Mg^{2+}]$ returned to the original seawater level, indicating that previously precipitated $Mg(OH)_2$ had fully dissolved $[Ca^{2+}]$ initially decreased, then increased, with an overall slight rise from a low of 22,006 μM to around 26,217 μM. The pH drop slowed significantly during this phase, suggesting rapid dissolution of precipitated $CaCO_3$ (Eq. (8)). During the dissolution of the $CaCO_3$ layer, the underlying CaO is likely exposed and continues to dissolve. The synergistic action of $CaCO_3$ dissolution and CaO exposure leads to a slight recovery of $[Ca^{2+}]$ in the solution.

The chemical reactions involved in the process are as follows:

$$CaO + H_2O \rightarrow Ca^{2+} + 2OH^- \quad (6)$$

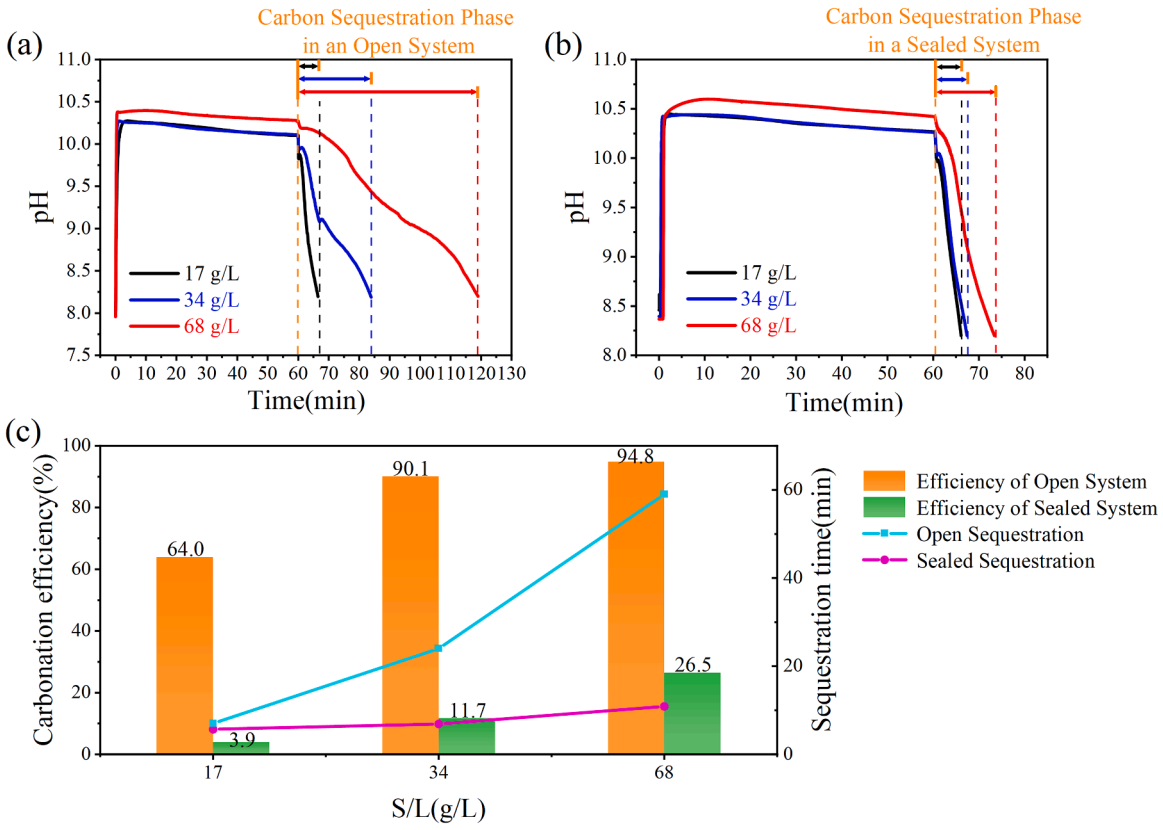


Fig. 2. (a) Time-dependent pH under different S/L (open); (b) Time-dependent pH under different S/L (sealed); (c) Carbonation efficiency and sequestration time under different S/L (open and sealed) [11].

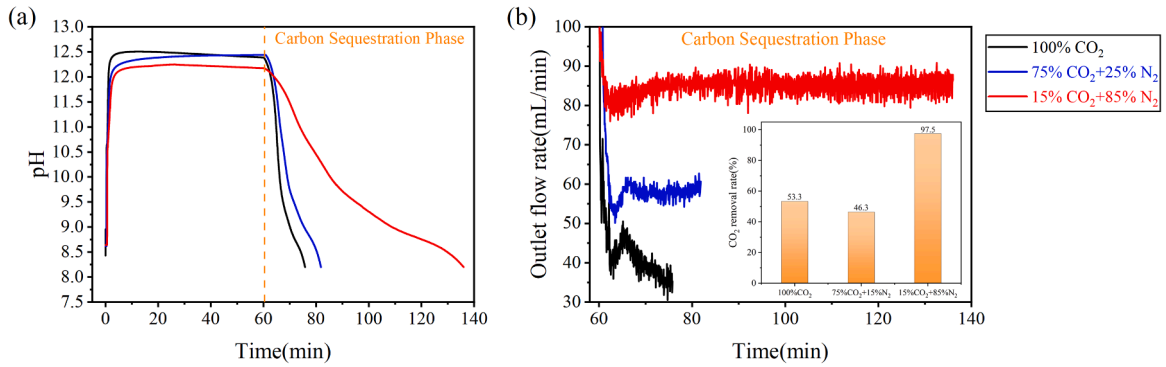


Fig. 3. Experimental results under different gas purities:(a) pH variation over time;(b) Outlet flow rate variation over time and CO_2 removal rate.

$$Ca^{2+}+2OH^{-}+CO_2 \rightarrow CaCO_3 + H_2O \quad (7)$$

$$CaCO_3 + H_2O + CO_2 \rightarrow Ca^{2+}+2HCO_3^{-} \quad (8)$$

$$Mg^{2+}+2OH^{-} \rightarrow Mg(OH)_2 \quad (9)$$

$$CO_2 + H_2O \rightleftharpoons H_2CO_3 \quad (10)$$

$$CO_2+OH^{-} \rightleftharpoons HCO_3^{-} \quad (11)$$

$$HCO_3^{-} \rightleftharpoons H^{+}+CO_3^{2-} \quad (12)$$

$$Mg(OH)_2+2H^{+} \rightarrow Mg^{2+}+2H_2O \quad (13)$$

After waiting at low pH for approximately 5 min, raw CFA was added to start the next cycle of experiments and achieve a new S/L. At the final cycle, CO_2 introduction was terminated as the solution's pH level dropped to 8.2.

3.3. Carbonation efficiency and CO_2 removal rate

TGA samples are taken from the solid carbonated CFA when the pH drops to 8.2 [34] and [Ca^{2+}] in the solution was at its minimum, indicating the end of the carbonation reaction in each cycle. The grey solid line in Fig. 5b illustrates the mass loss of the original CFA at 105 ℃, 105 ℃ - 600 ℃, and 600 ℃ - 950 ℃, revealing trace amounts of $Ca(OH)_2$ and $CaCO_3$ (0.768 wt %) in the original CFA. Since the $CaCO_3$ present in the original CFA does not participate in mineral carbonation, its decomposition weight loss must be deducted when calculating $SeCO_2$ and ζCa (%). It can be calculated that the actual CaO content in the original CFA in this study is approximately 7.272 wt %.

The outlet gas flow rate and TGA results for different cycles are shown in Fig. 5a and b. The CO_2 removal rate (Eq. (5)) and carbonation efficiency (Eq. (8)) for Cycles 1, 2, and 3 were 62.2 %, 66.9 %, and 80.3 %, and 26.5 %, 29.6 %, and 31.3 %, respectively. Both metrics increased significantly, as shown in Fig. 5c.

The SEM images of raw CFA and solids from three cycles are shown in Fig. 6. Fig. 6a shows raw CFA with smooth spherical particles, with EDS analysis revealing O as the dominant surface element, followed by Al, Ca, Si, and Fe. From Fig. 6b–d, irregular blocky crystals increase in density, transitioning to coarse needle-like structures in Fig. 6d EDS spot scanning confirms that these structures are primarily composed of O, C, and Ca, indicating $CaCO_3$ crystals. These SEM results visually demonstrate the enhanced carbonation efficiency with each cycle.

3.4. Comparative discussion and mechanism analysis

3.4.1. Comparative discussion

In recent years, significant progress has been made in improving the carbonation efficiency of CFA. Studies have found that supercritical conditions and open systems can both effectively enhance carbonation efficiency, mainly due to the significant increase in the leaching of CaO from CFA [11,32–34,45].

Under supercritical conditions, the high-temperature and high-pressure environment can activate the unreacted calcium in CFA, promoting the large-scale leaching of Ca^{2+} while maintaining the solubility of CO_2 in the liquid phase, thereby significantly improving carbonation efficiency [9,45]. However, this method has high energy consumption, which limits its widespread application in industry. In open systems, when using CFA and artificial seawater, the carbonation efficiency can reach 94.8 % [11], which is much higher than that in sealed systems. However, this method has obvious drawbacks: due to the open nature of the system, the escape of CO_2 is severe, and the escaped gas is difficult to collect and recycle. Moreover, the reaction time is too long, which is not conducive to industrial applications.

In contrast, under low-energy input (ambient temperature) conditions in a sealed system, the carbonation efficiency of CFA is usually low, generally not exceeding 31 %, which also indicates that the dissolution of CaO in CFA is not complete [32–34] (Table 1).

In Section 3.1, the reaction time and carbonation efficiency were compared between open and sealed systems. As shown in Fig. 2c, the difference in the duration of the carbonation phase between the two systems increases with higher S/L, rising from 1.5 min (17 g/L) to 50 min (68 g/L). Consequently, the carbonation efficiency difference exceeds 60 %. This discrepancy arises because, in the open system, excess CO_2 escapes into the environment, maintaining atmospheric pressure, while in the sealed system, unabsorbed CO_2 accumulates above the solution, increasing pCO_2. From a kinetic perspective, higher pCO_2 accelerates CO_2 dissolution, rapidly lowering the pH to 8.2, and promotes rapid $CaCO_3$ formation on CFA particle surfaces, hindering CaO leaching.

The CFA cyclic seawater carbonation method proposed in this study enhances the leaching of CaO from CFA by promoting the dissolution of $CaCO_3$ on the surface of CFA particles, thereby improving the carbonation efficiency and CO_2 removal rate in a sealed system, which will be discussed in detail in Section 3.4.2. This offers a new idea for the industrial application of CFA mineralization storage at room temperature.

3.4.2. Interfacial behavior of $CaCO_3$ during cyclic carbonation processes

During aeration, $CaCO_3$ crystals adhered to and grew on CFA particle surfaces (Fig. 6), consistent with previous studies [11]. CFA particles act as nucleation sites, lowering the energy required for $CaCO_3$ nucleation. This results in a dense $CaCO_3$ layer covering CFA particles, reducing their contact with the solution and hindering further CaO leaching.

[Ca^{2+}] in the solution during the aeration phase reaches a minimum and then increases shows that as CO_2 is continuously introduced, $CaCO_3$ precipitates including the portion on the CFA particle surfaces do dissolves (Eq. (8)). At this point, CFA particles regain direct contact with the liquid phase, and CaO leaching from CFA is no longer hindered by surface $CaCO_3$, allowing more CaO to dissolve. When the pH drops to

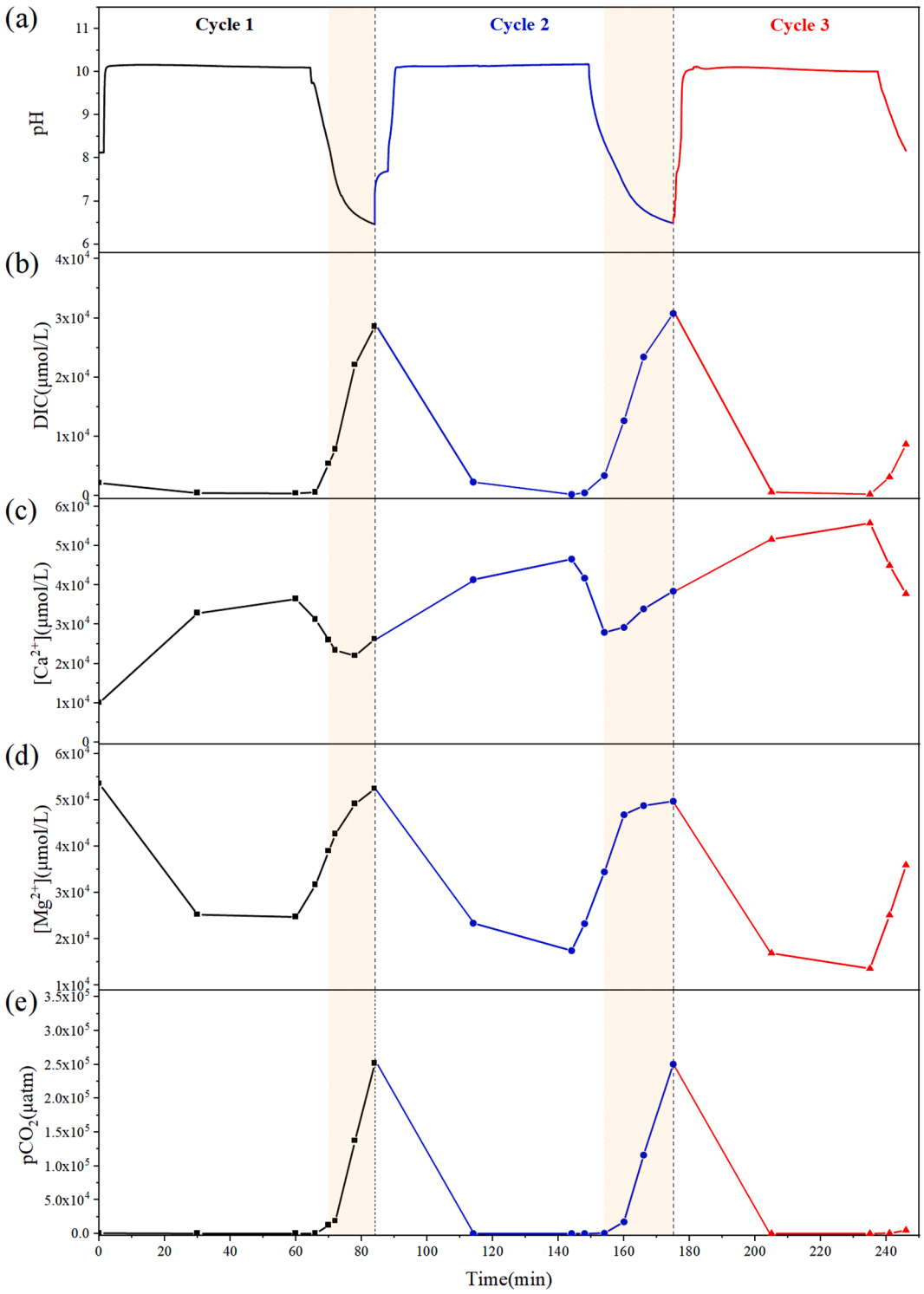


Fig. 4. Changes in pH (a), DIC (b), $[Ca^{2+}]$ (c), $[Mg^{2+}]$ (d) and pCO_2(e) in the solution over time in cyclic experiments. The pale yellow areas between 70 min - 84 min and 154 min - 175 min indicate the changes in solution parameters after the pH dropped to 8.2 and CO_2 was continuously introduced.

6.5, the CO_2 in the solution becomes supersaturated, leading to an excessively high pCO_2. At this stage, CaO in the newly added CFA stabilizes the excess CO_2 in the solution, while the acidic environment promotes CaO leaching from both the new CFA and any unreacted CaO in the original CFA. As the number of cycles increases, CaO leaching from CFA also rises, corresponding to the observed improvements in carbonation efficiency and CO_2 removal rates.

3.4.3. *Effect of S/L*

In the cyclic experiments, the S/L was adjusted from 68 g/L in Cycle 1 to 204 g/L and 340 g/L in Cycles 2 and 3, respectively, by adding more CFA. This change likely significantly impacted carbonation efficiency.To study the impact of S/L on carbonation efficiency, experiments were conducted at S/L of 17, 34, 68, and 136 g/L, with other conditions consistent with the cyclic experiments.

All groups exhibited similar trends (Figs. 7 and 8). Adding CFA

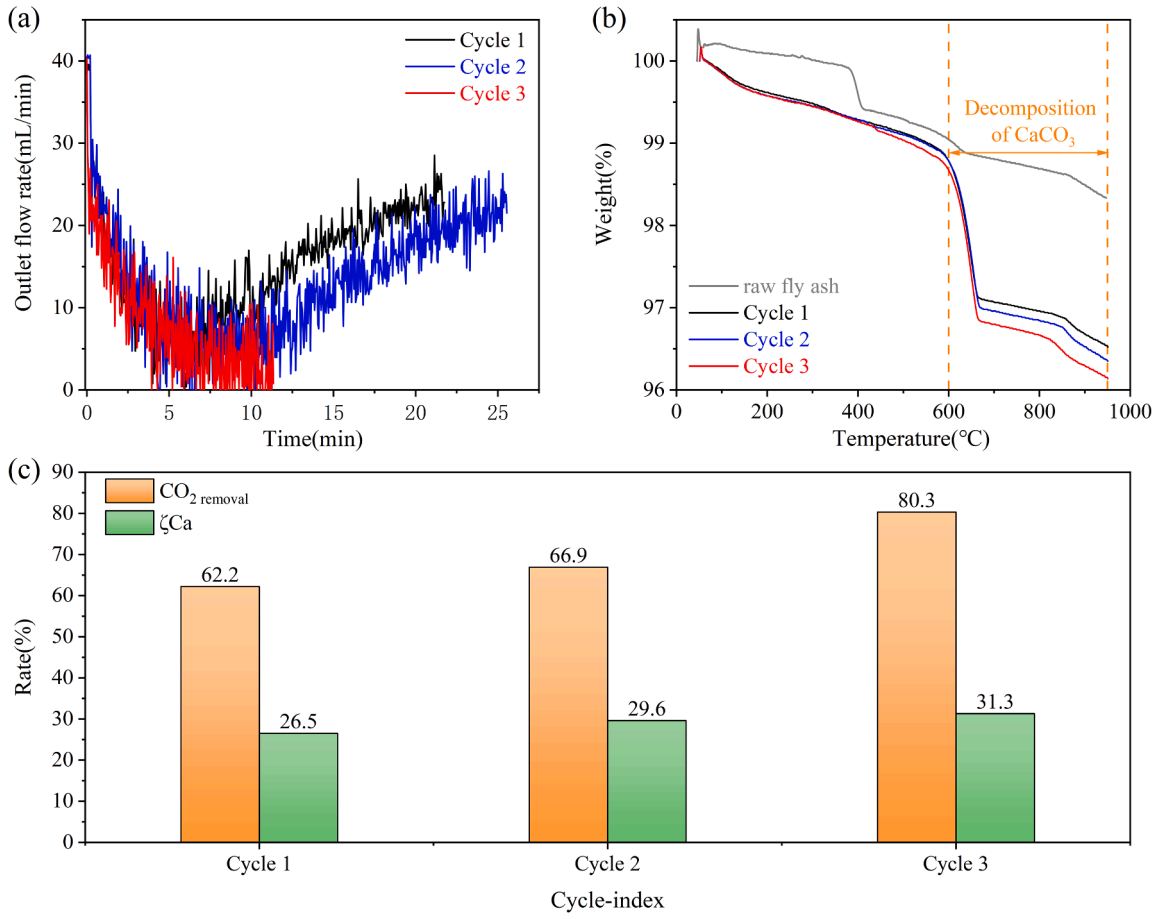


Fig. 5. (a)Variation of outlet gas flow rate over time in the cyclic CFA experiment. (b)TGA curves of the raw CFA and the carbonated CFA after different cycles of carbonation. (c)Carbonation efficiency (ζCa(%)) of CFA and the CO_2 removal rate ($CO_{2removal}$) in the cyclic experiment.

rapidly increased the pH above 10.4, accompanied by a surge in [Ca^{2+}], indicating CaO dissolution. During activation, [Mg^{2+}] decreased with a slight pH drop, suggesting $Mg(OH)_2$ precipitation. DIC declined as Ca^{2+} utilized seawater DIC for $CaCO_3$ formation. During aeration, pH gradually decreased, while [Ca^{2+}] initially dropped sharply before rebounding (Fig. 8) [Mg^{2+}] increased steadily, and DIC accumulated, indicating three processes: (1) CO_2 dissolution and $Mg(OH)_2$ resolubilization, (2) partial CO_2 hydrolysis forming and dissolving $CaCO_3$, and (3) CO_2 integration into seawater as DIC.

Based on Eqs. (3) and 5 (Fig. 9b), the CO_2 removal rates and carbonation efficiencies increased with the S/L, showing a positive correlation. At S/L of 17, 34, 68, and 136 g/L, the CO_2 removal rates were 54 %, 64 %, 68 %, and 78 %, and the carbonation efficiencies were 3.9 %, 11.7 %, 19.7 %, and 24.7 %, respectively. This aligns with the findings of Ho et al. [33]. Higher S/L required longer times to reach the target pH under constant gas flow (Fig. 9a). Similarly, at high CO_2 flow rates, the rapid decrease in pH cannot be fully counterbalanced by the pH increase resulting from CaO dissolution, leading to shorter reaction times and incomplete extraction of CaO. Increased S/L enhances CaO content, boosting Ca dissolution and aeration time, thus improving carbonation efficiency and CO_2 removal.

The S/L experiment shows that increasing the S/L can extend the time to reach the pH reaction endpoint, thereby enhancing CO_2 removal rate and carbonation efficiency. The CFA circulating seawater carbonation experiment employed a repeated cycling strategy to increase the system S/L, progressively extending the aeration time (5.7, 6.0, and 8.8 min for three cycles), achieving simultaneous improvement in both carbonation efficiency and CO_2 removal rate. However, excessively high S/L inhibits CaO leaching due to insufficient solution, leading to reduced carbonation efficiency and CO_2 removal rate, thus imposing an upper limit on the number of cycles.

3.4.4. *Effect of Mg/Ca*

The Mg/Ca in seawater significantly impacts the kinetics and crystallography of $CaCO_3$ precipitation [46]. During the cyclic experiments, [Ca^{2+}] increases progressively due to CaO dissolution, reducing the Mg/Ca and potentially affecting carbonation efficiency. (Mg^{2+} mainly comes from seawater, while CFA contains negligible Mg.) To study this effect, we substituted CFA with pure CaO as the Ca^{2+} source and prepared artificial seawater with Mg/Ca = 0, 5, and 7.5 for CO_2 mineralization, keeping other conditions identical to the cyclic seawater carbonation experiments.

Fig. S1 shows the changes in [Ca^{2+}], [Mg^{2+}], and DIC in artificial seawater with initial Mg/Ca of 0, 5, and 7.5. During stirring activation, [Ca^{2+}] increased and DIC decreased due to CaO dissolution (Eq. (6)) [Mg^{2+}] decreased for $Mg(OH)_2$ precipitation (Eq. (9)) in Mg-containing groups, lowering Mg/Ca. After activation, the Mg/Ca became 0, 1.8, and 3.2 for the initial values of 0, 5, and 7.5, respectively. After 15 min of CO_2 introduction, [Ca^{2+}] reductions were 10,474, 5757, and 3365 μmol/L for initial Mg/Ca of 0, 5, and 7.5. Final CO_2 removal efficiencies were 52.2 %, 44.4 %, and 32.7 %. (Fig. 10). This indicates that higher Mg/Ca result in smaller decreases in [Ca^{2+}] during the reaction, leading to less $CaCO_3$ formation and lower CO_2 removal rates.

Mg^{2+} and Ca^{2+} are both non-transition metal divalent cations with similar ionic properties, which allows Mg^{2+} to incorporate into the calcite lattice and adsorb at specific lattice sites [46,47]. However, due to the different ionic sizes of Mg^{2+} and Ca^{2+}, this adsorption process increases the surface energy barrier required for $CaCO_3$ nucleation,

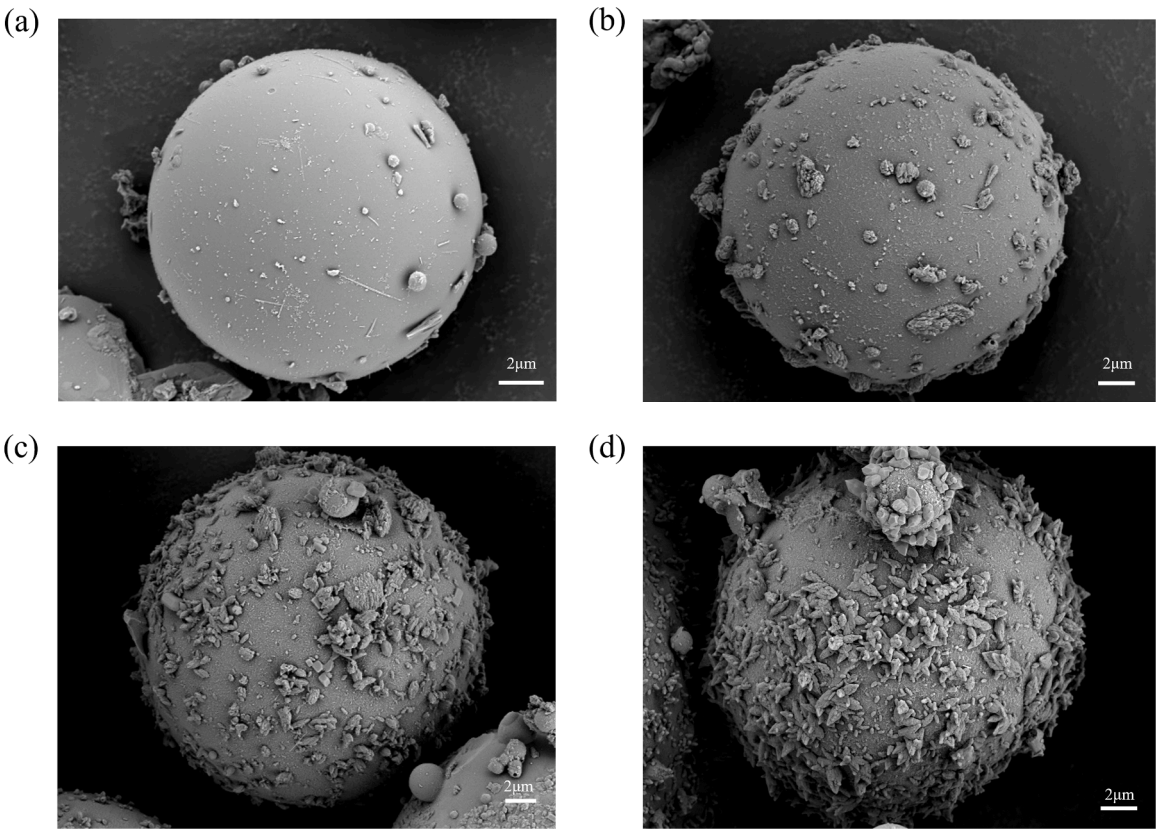


Fig. 6. SEM images of (a) the raw CFA, (b) the carbonized sample in Cycle 1, (c) the carbonized sample in Cycle 2, (d) the carbonized sample in Cycle 3.

Table 1
Comparison of CO_2 sequestration capacity ($SeCO_2$) and carbonation efficiency (ζCa(%)) between this study and previous studies under ambient temperature and pressure conditions.

	Effective CaO	Solvent	$SeCO_2$(kg CO_2/ t CFA)	S/L (g/ L)	ζCa (%)	References
Raw fly ash	7.2 wt. %	DI	8.0	100	5.0	Jo et al.,2012a [34]
Raw fly ash	7.2 wt. %	Seawater	19.0	333	29.2	Jo et al.,2012b [32]
Raw fly ash	4.23 wt. %	DI	17.4	50	18.0	Han et al.,2015 [35]
Raw fly ash	3.44 wt. %	DI	6.3	10	31.0	Ho et al.,2021 [33]
Raw fly ash	7.272 wt. %	Seawater	49.2	68	94.8	Ding et al.,2023 [11]
			14.9	68	26.5	This work
			16.6	204	29.6	
			17.6	340	31.3	

making calcite nucleation more difficult and thus inhibiting its crystallization [48]. Therefore, as the initial Mg/Ca increases, the crystallization of $CaCO_3$ is suppressed, resulting in a smaller decrease in [Ca^{2+}] during the reaction, ultimately reducing the formation of $CaCO_3$ and lowering the CO_2 removal efficiency [46]. Additionally, higher Mg/Ca also promote the conversion of calcite to aragonite (Fig. 11).

In the S/L experiment, Mg/Ca varied between 0 and 5.2 with pH changes. After activation, Mg/Ca decreased from 5.2 to 3.0, 1.6, 0.6, and 0 in the 17, 34, 68, and 136 g/L groups, respectively. This further explains the higher carbonation efficiency at higher S/L.

In the cyclic experiments, the Mg/Ca in the solution changes with the increase in the number of cycles. The Mg/Ca following activation in Cycle 1, Cycle 2, and Cycle 3 were 2.9, 0.4, and 0.2, respectively. With an increase in the number of cycles, [Ca^{2+}] in the solution escalates during the activation phase of each cycle due to the sustained dissolution of CaO from the CFA. Concurrently, $Mg(OH)_2$ precipitations in the high pH environment of the activation phase leads to a phased reduction in [Mg^{2+}]. As a result, the Mg/Ca in the solution post-activation of each cycle diminishes incrementally with the progression of cycle repetitions.

The decrease in Mg/Ca during the cycles explains the improved carbonation efficiency and CO_2 removal rate. As the cycles progress, Mg/Ca decreases after activation, reducing the inhibition of $CaCO_3$ crystallization and accelerating CO_2 conversion to $CaCO_3$, thereby enhancing carbonation efficiency and CO_2 removal.

Based on the mechanistic discussions of the cyclic carbonation process (Sections 3.4.1–3.4.4), Fig. 12 integrates the core mechanisms and their interactions that enhance the carbonation efficiency of CFA under the cyclic strategy, including the periodic dissolution and reprecipitation of surface $CaCO_3$, the cumulative effect of S/L, and the positive impact of progressively decreasing Mg/Ca on crystallization kinetics. In the figure, "+" denotes promoting effects and "–" denotes inhibiting effects.

3.5. Cost analysis

The economic viability and energy efficiency of aqueous mineral carbonation of CFA must be carefully evaluated. While seawater is inexpensive, pumping it requires significant energy. Previous studies have set the S/L at 10 g/L - 100 g/L [33–35], meaning 10^4 m^3 - 10^5 m^3 of seawater is needed per 1000 t of CFA. In 2021, Chinese thermal power plants generated approximately 1.6 Mt of CFA daily [49,50]. Using all this CFA for mineral carbonation would require pumping 1.6×10^7 m^3

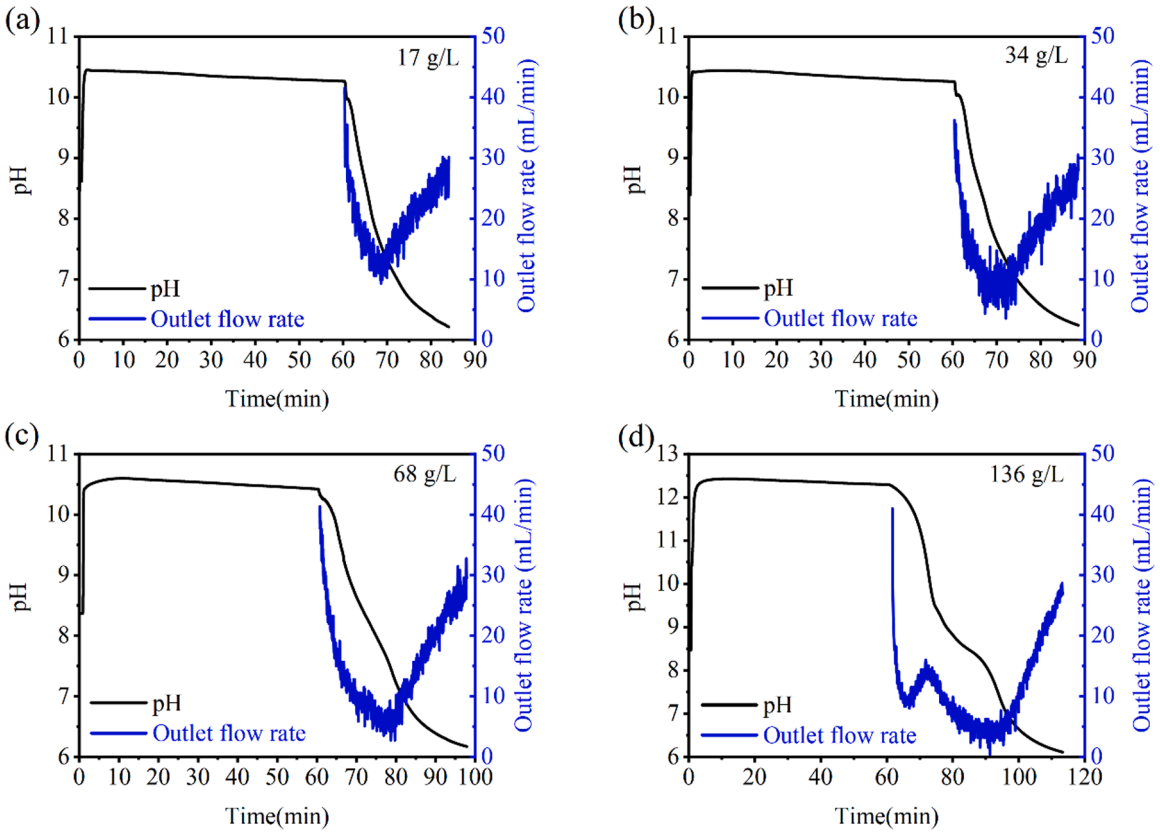


Fig. 7. The temporal variations in pH and outlet gas flow rate for CFA groups with different S/L (17, 34, 68, and 136 g/L).

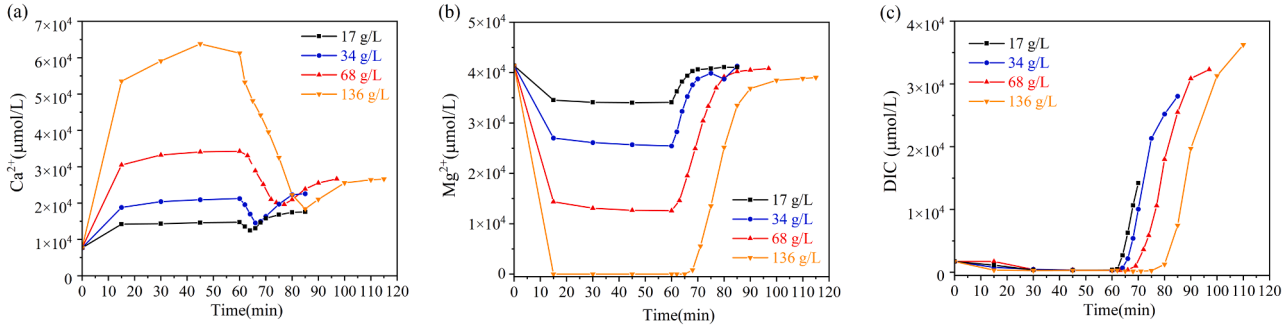


Fig. 8. The variations in $[Ca^{2+}]$, $[Mg^{2+}]$, and DIC concentrations over time for CFA groups with S/L of 17, 34, 68, and 136 g/L.

to 1.6×10^8 m^3 of seawater. Taking the pumps at Zhanjiang Power Plant as an example [51], this would entail an energy consumption ranging from 1.07×10^6 kWh to 1.07×10^7 kWh. With the electricity price for large industrial consumers in Zhejiang Province set at 0.09 USD/kWh [52], the energy expenditure solely for seawater pumping could reach between 96,300 USD and 963,000 USD. While it is unrealistic to use all CFA for carbonation in actual industrial production, this highlights the significant energy costs associated with pumping seawater. The cyclic seawater carbonation method increases S/L without additional seawater pumping, maintaining efficiency even at 340 g/L. This reduces seawater pumping energy consumption to one-third to one-thirtieth of that required for S/L of 10 g/L - 100 g/L, lowering CO_2 sequestration costs.

Furthermore, carbonated CFA can serve as a supplementary cementitious material, offering broader applications and higher economic value than raw CFA. Wei et al. demonstrated that carbonated CFA enhances the strength of cement-CFA mixtures, with strength increasing proportionally to CO_2 absorption [31]. Compared to raw CFA, carbonated CFA has lower f-CaO content, addressing durability issues in cement-based materials. This reduction results from f-CaO consumption during carbonation and the formation of a dense $CaCO_3$ layer encapsulating f-CaO. Carbonated CFA is an environmentally friendly product, and its enhanced economic value can partially offset the treatment costs, providing new possibilities for achieving a win-win situation in terms of economic and environmental benefits (Table 2).

Additionally, given the potential cost increase associated with heavy metal treatment after the cycles, we analyzed the possibility of heavy metal enrichment. Leaching tests for heavy metals in CFA from prior studies showed that the leaching concentrations of all major heavy metals were significantly below the regulatory limits (Chinese National Standard GB 18,486–2001) [11,53]. This aligns with findings on CFA leaching behavior reported by Ukwattage et al. [54] and Yuan et al. [55]. Although multiple cycles might lead to an accumulation of heavy metal elements in the solution, mechanistically, the carbonation process (conversion of CaO to precipitated $CaCO_3$) exhibits significant co-precipitation and immobilization effects on many heavy metal elements [55]. Therefore, CFA carbonation essentially helps reduce its

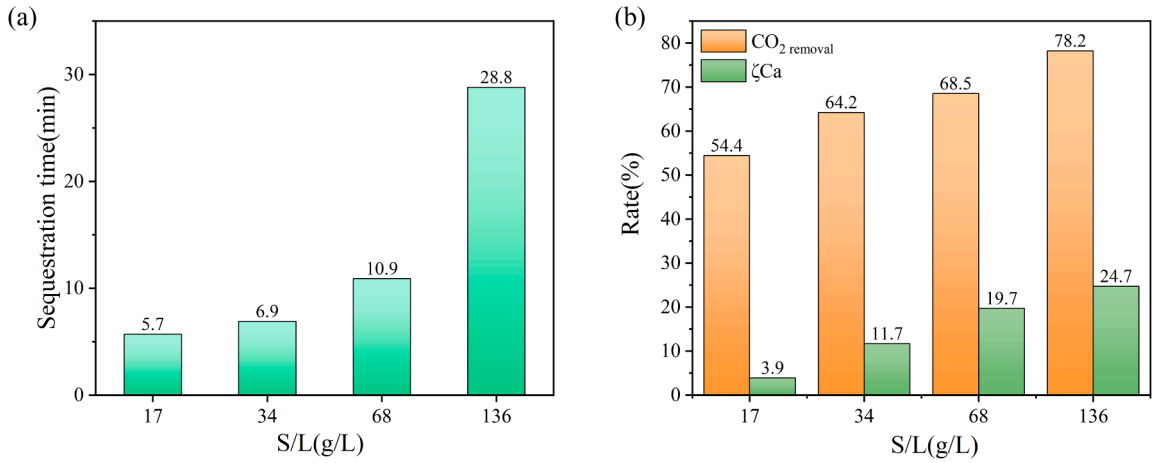


Fig. 9. (a)The aeration time of CFA at different S/L.(b) The carbon fixation efficiency (ζCa %) and CO_2 removal rate ($CO_{2removal}$) in CFA groups with different S/L.

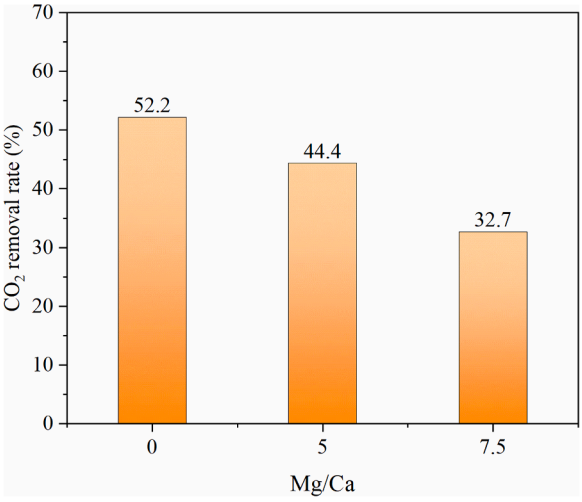


Fig. 10. CO_2 removal rate ($CO_{2removal}$) with different initial Mg/Ca.

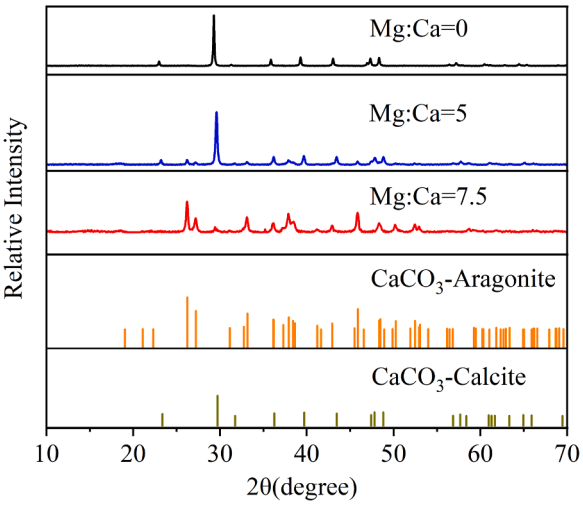


Fig. 11. XRD of Aragonite (standard card PDF#75–2230), Calcite (standard card PDF#72–1937), and solid samples taken after introducing CO_2 gas under different Mg/Ca(0, 5, 7.5) until the system pH reaches 8.2.

toxicity. Our cyclic method is designed to gradually enhance the carbonation efficiency of CFA, which is expected to effectively control the overall leaching risk of heavy metals during multiple cycles. Given the importance of this issue, experimental verification will be needed in the future, focusing on monitoring and validating the above inferences during multiple cycles.

4. Conclusion

This study explores the potential of cyclic seawater mineralization for carbon sequestration in coastal coal-fired power plants, focusing on the application of a sealed system to meet industrial needs for dust containment and gas collection. The key conclusions are as follows:

(1) **Sealed vs. Open Systems**: Carbonation efficiency in sealed systems (26.5 %) is significantly lower than in open systems (94.8 %) under ambient conditions. Higher pCO_2 accelerates CO_2 dissolution, lowering the pH to 8.2 and promoting rapid $CaCO_3$ formation on CFA particles, hindering CaO leaching and reducing efficiency.

(2) **Cyclic Seawater Carbonation**: This method enhances carbonation efficiency from 26.5 % to 31.3 % and CO_2 removal from 62.2 % to 80.3 % in sealed, room-temperature systems. It offers energy savings, prevents dust leakage, and enables exhaust gas collection, providing an efficient carbon capture solution for coastal power plants.

(3) **Mechanisms**: Three mechanisms enhance carbonation: (i) cyclic processes dissolve surface $CaCO_3$, accelerating CaO leaching; (ii) higher S/L extends reaction time, enhancing CaO leaching; (iii) lower Mg/Ca reduces Mg^{2+} inhibition, speeding up $CaCO_3$ precipitation.

(4) **Economic and Environmental Benefits**: The method is sustainable and cost-effective, reducing infrastructure and operational costs by reusing seawater. The resulting carbonated CFA is a high-value cementitious material, offering greater economic benefits than raw CFA.

In summary, this study demonstrates how system design and reaction conditions optimize carbonation. The cyclic seawater carbonation method offers a promising approach to enhance CO_2 capture, contributing to global climate change mitigation and net-zero emission goals. Future research will aim to scale up this process for industrial implementation, incorporating monitoring of heavy metal leaching risks during operation.

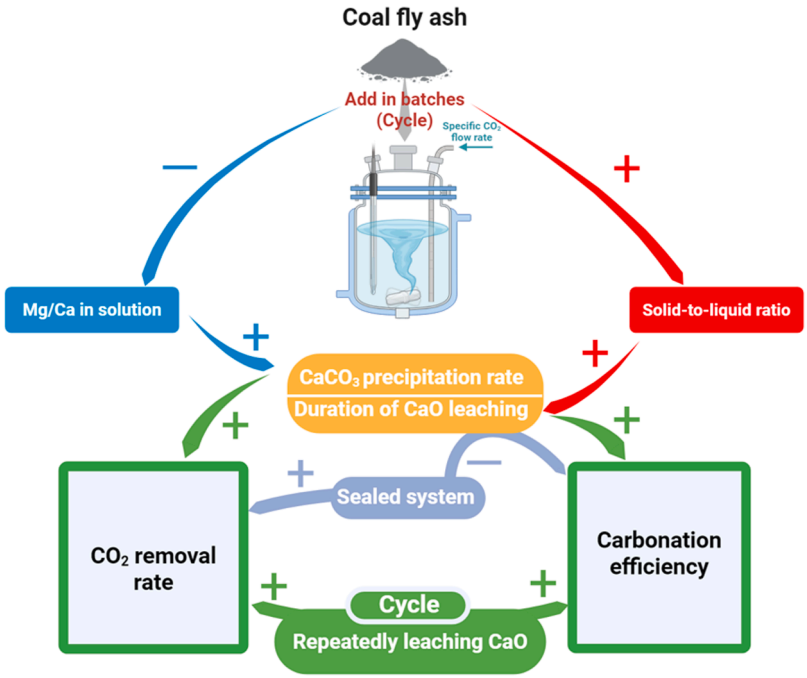


Fig. 12. Schematic of interaction mechanisms in CFA cyclic carbonation. Key: + promotion; - inhibition.

Table 2
Comparison of seawater pumping costs in conventional (literature [33–35]) and cyclic carbonation (this study).

	CFA used (t)	Seawater used (m3)	Pumping energy (kWh)	Pumping cost (USD)
Previous studies [33–35]	1000	104 - 105	670 - 6700	60 - 600
This study		2914	195	18

CRediT authorship contribution statement

Tianle Cheng: Writing – original draft, Data curation, Methodology, Investigation, Visualization. **Zesheng Ding:** Methodology, Investigation, Validation. **Xu Zhang:** Conceptualization, Methodology, Investigation. **Jiajun Chai:** Validation. **Yunwen Shen:** Methodology, Validation. **Lihong Cai:** Writing – review & editing. **Rui Bao:** Writing – review & editing. **Ying Chen:** Project administration. **Yiwen Pan:** Investigation, Formal analysis, Writing – review & editing, Conceptualization, Funding acquisition.

Declaration of competing interest

The authors declare that they have no known competing financial interests or personal relationships that could have appeared to influence the work reported in this paper.

Acknowledgements

The authors would be thankful to the laboratory technician Yuxia Sun for the help in element measurements. This work was supported by the National Natural Science Foundation of China (grants 42176036 and 42188102), the Zhejiang Provincial Department of Agriculture and Rural Affairs Science and Technology Cooperation Project (grant 2024SNJF054), the Science and Technology Program of Shengsi County (grant No.2023-03), Guangxi Key Laboratory of Beibu Gulf Marine Resources, Environment and Sustainable Development (grant MRESD-2022-A02), the Fundamental Research Funds for the Central Universities, and the Ocean Negative Carbon Emission (ONCE) program.

Supplementary materials

The following are the Supplementary data to this article: Supplementary Data 1.

Supplementary material associated with this article can be found, in the online version, at doi:10.1016/j.cep.2025.110428.

Data availability

Data will be made available on request.

References

[1] P. Friedlingstein, M. O'Sullivan, M.W. Jones, R.M. Andrew, L. Gregor, J. Hauck, et al., Global Carbon Budget 2022, Earth Syst. Sci. Data 14 (11) (2022) 4811–4900, https://doi.org/10.5194/essd-14-4811-2022.
[2] P. Friedlingstein, M. O'Sullivan, M.W. Jones, R.M. Andrew, D.C.E. Bakker, J. Hauck, et al., Global Carbon Budget 2023, Earth. Syst. Sci. Data 15 (12) (2023) 5301–5369, https://doi.org/10.5194/essd-15-5301-2023.
[3] S. Huang, J. Yuan, Supporting dual goals of energy supply and carbon reduction through low-carbon transformation of thermal power, Guangxi Electr. Power (12) (2022) 59–62, in Chinese.
[4] Q. Li, N. Liu, The discussion of coal companies' Transition pathway under the backgrounds of peak carbon and carbon neutrality, Coal Econ. Res. 41 (07) (2021) 45–51, https://doi.org/10.13202/j.cnki.cer.2021.07.006, in Chinese.
[5] C. Ye, Coal power transition and reconstruction under the Carbon neutrality target of the 14th five-year plan, China Power Enterp. Manag. (07) (2021) 17–21, in Chinese.
[6] J. Xi, Address at the general debate of the 75th session of the United Nations General Assembly, Bull. State Counc. People's Repub. China (28) (2020) 5–7, in Chinese.
[7] K.S. Lackner, A guide to CO_2 sequestration, Science 300 (5626) (2003) 1677–1678, https://doi.org/10.1126/science.1079033.
[8] A.A. Olajire, A review of mineral carbonation technology in sequestration of CO_2, J. Pet. Sci. Eng. 109 (2013) 364–392, https://doi.org/10.1016/j.petrol.2013.03.013.
[9] M.G. Nyambura, G.W. Mugera, P.L. Felicia, N.P. Gathura, Carbonation of brine impacted fractionated coal fly ash: implications for CO_2 sequestration, J. Environ. Manage. 92 (3) (2011) 655–664, https://doi.org/10.1016/j.jenvman.2010.10.008.
[10] H. Hou, L. Su, D. Guo, H. Xu, Resource utilization of solid waste for the collaborative reduction of pollution and carbon emissions: case study of fly ash, J. Clean. Prod. 383 (2023) 135449, https://doi.org/10.1016/j.jclepro.2022.135449.
[11] Z. Ding, X. Zhang, T. Cheng, Y. Shen, W.-J. Cai, C.-T. Arthur Chen, et al., Unlocking high carbonation efficiency: direct CO_2 mineralization with fly ash and seawater, Chem. Eng. Sci. 282 (2023) 119349, https://doi.org/10.1016/j.ces.2023.119349.

[12] H. Li, R. Zhang, T. Wang, Y. Wu, R. Xu, Q. Wang, et al., Performance evaluation and environment risk assessment of steel slag enhancement for seawater to capture CO_2, Energy 238 (2022) 121861, https://doi.org/10.1016/j.energy.2021.121861.
[13] E. Ren, S. Tang, C. Liu, H. Yue, C. Li, B. Liang, Carbon dioxide mineralization for the disposition of blast-furnace slag: reaction intensification using NaCl solutions. Greenhouse gases, Sci. Technol. 10 (2) (2018) 436–448, https://doi.org/10.1002/ghg.1837.
[14] S. Eloneva, S. Teir, J. Salminen, C.-J. Fogelholm, R. Zevenhoven, Fixation of CO_2 by carbonating calcium derived from blast furnace slag, Energy 33 (9) (2008) 1461–1467, https://doi.org/10.1016/j.energy.2008.05.003.
[15] A. Uliasz-Bocheńczyk, J. Deja, Potential application of cement kiln dust in carbon capture, utilisation, and storage technology, Energy 292 (2024) 130412, https://doi.org/10.1016/j.energy.2024.130412.
[16] S.K. Adekunle, Carbon sequestration potential of cement kiln dust: mechanisms, methodologies, and applications, J. Clean. Prod. 446 (2024) 141283, https://doi.org/10.1016/j.jclepro.2024.141283.
[17] Q. Zhang, P. Feng, X. Shen, J. Lu, S. Ye, H. Wang, et al., Utilization of solid wastes to sequestrate carbon dioxide in cement-based materials and methods to improve carbonation degree: a review, J. CO_2 Util. 72 (2023) 102502, https://doi.org/10.1016/j.jcou.2023.102502.
[18] A. Rita Damasceno Costa, J. Pereira Gonçalves, Accelerated carbonation of ternary cements containing waste materials, Constr. Build. Mater. 302 (2021) 124159, https://doi.org/10.1016/j.conbuildmat.2021.124159.
[19] D-H Vu, H.-B. Bui, B. Kalantar, X.-N. Bui, D-A Nguyen, Q.-T. Le, et al., Composition and morphology characteristics of magnetic fractions of coal fly ash wastes processed in high-temperature exposure in thermal power plants, Appl. Sci. 9 (9) (2019) 1964, https://doi.org/10.3390/app9091964.
[20] X. Sun, A. Shang, P. Wu, T. Liu, Y. Li, A review of CO_2 Marine geological sequestration, Processes 11 (7) (2023) 2206, https://doi.org/10.3390/pr11072206.
[21] A.R.K. Gollakota, V. Volli, C.-M. Shu, Progressive utilisation prospects of coal fly ash: a review, Sci. Total Environ. 672 (2019) 951–989, https://doi.org/10.1016/j.scitotenv.2019.03.337.
[22] Z.T. Yao, X.S. Ji, P.K. Sarker, J.H. Tang, L.Q. Ge, M.S. Xia, et al., A comprehensive review on the applications of coal fly ash, Earth-Sci. Rev. 141 (2015) 105–121, https://doi.org/10.1016/j.earscirev.2014.11.016.
[23] H.-J. Ho, A. Iizuka, Mineral carbonation using seawater for CO2 sequestration and utilization: a review, Sep. Purif. Technol. 307 (2023) 122855, https://doi.org/10.1016/j.seppur.2022.122855.
[24] A. Dindi, D.V. Quang, L.F. Vega, E. Nashef, M.R.M. Abu-Zahra, Applications of fly ash for CO_2 capture, utilization, and storage, J. CO_2 Util. 29 (2019) 82–102, https://doi.org/10.1016/j.jcou.2018.11.011.
[25] Y. Soong, D.L. Fauth, B.H. Howard, J.R. Jones, D.K. Harrison, A.L. Goodman, et al., CO_2 sequestration with brine solution and fly ashes, Energy Convers. Manag. 47 (13–14) (2006) 1676–1685, https://doi.org/10.1016/j.enconman.2005.10.021.
[26] M. Back, M. Kuehn, H. Stanjek, S. Peiffer, Reactivity of alkaline lignite fly ashes towards CO_2 in water, Env. Sci. Technol. 42 (12) (2008) 4520–4526, https://doi.org/10.1021/es702760v.
[27] M. Kim, J. Na, S. Park, J.-H. Park, C. Han, Modeling and validation of a pilot-scale aqueous mineral carbonation reactor for carbon capture using computational fluid dynamics, Chem. Eng. Sci. 177 (2018) 301–312, https://doi.org/10.1016/j.ces.2017.11.033.
[28] N. Czaplicka, D. Konopacka-Łyskawa, The overview of reactors used for the production of precipitated calcium carbonate via carbonation route, Apar. Badaw. Dydakt. 24 (1) (2019) 83–90.
[29] S.-Y. Pan, Y.-H. Chen, L-S Fan, H. Kim, X. Gao, T.-C. Ling, et al., CO_2 mineralization and utilization by alkaline solid wastes for potential carbon reduction, Nat. Sustain. 3 (5) (2020) 399–405, https://doi.org/10.1038/s41893-020-0486-9.
[30] K. Rausis, A. Ćwik, I. Casanova, K. Zarębska, Carbonation of high-Ca fly ashes under flue gas conditions: implications for their valorization in the construction industry, Crystals 11 (11) (2021) 1314, https://doi.org/10.3390/cryst11111314.
[31] Z. Wei, B. Wang, G. Falzone, E.C. La Plante, M.U. Okoronkwo, Z. She, et al., Clinkering-free cementation by fly ash carbonation, J. CO_2 Util. 23 (2018) 117–127, https://doi.org/10.1016/j.jcou.2017.11.005.
[32] H.Y. Jo, J.-H. Ahn, H. Jo, Evaluation of the CO_2 sequestration capacity for coal fly ash using a flow-through column reactor under ambient conditions, J. Hazard. Mater. 241-242 (2012) 127–136, https://doi.org/10.1016/j.jhazmat.2012.09.020.
[33] H.-J. Ho, A. Iizuka, E. Shibata, Utilization of low-calcium fly ash via direct aqueous carbonation with a low-energy input: determination of carbonation reaction and evaluation of the potential for CO_2 sequestration and utilization, J. Environ. Manage. 288 (2021) 112411, https://doi.org/10.1016/j.jenvman.2021.112411.
[34] H.Y. Jo, J.H. Kim, Y.J. Lee, M. Lee, S.-J. Choh, Evaluation of factors affecting mineral carbonation of CO_2 using coal fly ash in aqueous solutions under ambient conditions, Chem. Eng. J. 183 (2012) 77–87, https://doi.org/10.1016/j.cej.2011.12.023.
[35] S.-J. Han, H.J. Im, J.-H. Wee, Leaching and indirect mineral carbonation performance of coal fly ash-water solution system, Appl. Energy 142 (2015) 274–282, https://doi.org/10.1016/j.apenergy.2014.12.074.
[36] China MoEaEotPsRo. Comprehensive plan for the integrated control of air pollution from industrial furnaces and kilns; 2019. Available from: https://www.gov.cn/zhengce/zhengceku/2019-11/25/content_5455426.htm [Accessed 01-25 2025].
[37] J. Cai, Z. Li, First principle-based rate equation theory for the carbonation kinetics of CaO with CO_2 in calcium looping, Chem. Eng. J. 479 (2024) 147484, https://doi.org/10.1016/j.cej.2023.147484.
[38] S.A. Salaudeen, B. Acharya, A. Dutta, CaO-based CO_2 sorbents: a review on screening, enhancement, cyclic stability, regeneration and kinetics modelling, J. CO_2 Util. 23 (2018) 179–199, https://doi.org/10.1016/j.jcou.2017.11.012.
[39] L. Li, M. Wu, An overview of utilizing CO2 for accelerated carbonation treatment in the concrete industry, J. CO_2 Util. 60 (2022), https://doi.org/10.1016/j.jcou.2022.102000.
[40] D. Zhang, V.C. Li, B.R. Ellis, Optimal pre-hydration age for CO2 sequestration through Portland cement carbonation, ACS. Sustain. Chem. Eng. 6 (12) (2018) 15976–15981, https://doi.org/10.1021/acssuschemeng.8b03699.
[41] Y. Pan, Z. Sun, H. He, Y. Li, L. You, H. Zheng, An improved method of preparing iridium oxide electrode based on carbonate-melt oxidation mechanism, Sens. Actuators B: Chem. 261 (2018) 316–324, https://doi.org/10.1016/j.snb.2018.01.069.
[42] Z. Sun, Q. Ma, Y. Wang, Y. Pan, Effects of structures on the sensing properties of long-term stable IrOx pH electrodes, J. Electrochem. Soc. 167 (4) (2020) 047501, https://doi.org/10.1149/1945-7111/ab717e.
[43] E. Lewis, D. Wallace, L.J. Allison, Program Developed For CO_2 System calculations. Brookhaven National Lab., Dept. of Applied Science, Upton, NY(United States), Oak Ridge National Lab., Carbon Dioxide Information Analysis Center, TN(United States), 1998.
[44] L. Ji, H. Yu, X. Wang, M. Grigore, D. French, Y.M. Gözükara, et al., CO_2 sequestration by direct mineralisation using fly ash from Chinese Shenfu coal, Fuel Process. Technol. 156 (2017) 429–437, https://doi.org/10.1016/j.fuproc.2016.10.004.
[45] A. Ćwik, I. Casanova, K. Rausis, K. Zarębska, Utilization of high-calcium fly ashes through mineral carbonation: the cases for Greece, Poland and Spain, J. CO_2 Util. 32 (2019) 155–162, https://doi.org/10.1016/j.jcou.2019.03.020.
[46] Y. Pan, Y. Li, Q. Ma, H. He, S. Wang, Z. Sun, et al., The role of Mg^{2+} in inhibiting $CaCO_3$ precipitation from seawater, Mar. Chem. 237 (2021) 104036, https://doi.org/10.1016/j.marchem.2021.104036.
[47] W. Feng, Z.Y. Ng, H. Chen, J. Zhang, D. Xu, Y. He, et al., Calcium ion deposition with precipitated Calcium carbonate: influencing factors and mechanism exploration, Processes 12 (4) (2024) 629, https://doi.org/10.3390/pr12040629.
[48] W. Sun, S. Jayaraman, W. Chen, K.A. Persson, G. Ceder, Nucleation of metastable aragonite $CaCO_3$ in seawater, Proc. Natl. Acad. Sci. 112 (11) (2015) 3199–3204, https://doi.org/10.1073/pnas.1423898112.
[49] China NBoSo, China Statistical Yearbook 2023, 2023. Available from: https://www.stats.gov.cn/sj/ndsj/2023/indexch.htm [Accessed 06-20 2024].
[50] Government NPsM. 2023 Review and outlook on the comprehensive utilization of bulk industrial solid waste; 2023. Available from: https://www.np.gov.cn/cms/html/npszf/2023-12-20/1215591946.html [Accessed 06-20 2024].
[51] G. Zhen, Condition analysis and optimization retrofit plan for circulating water pumps in thermal power plants, Pump Technol. (01) (2015) 38–40, in Chinese.
[52] S. Grid, Notice On the Electricity Purchase Price for Agency Industrial and Commercial Users in June 2024 By State Grid Zhejiang Electric Power Co., Ltd, 2024. Available from: https://www.zj.sgcc.com.cn/p1/djmljsfbz.html [Accessed 06-20 2024].
[53] China MoEaEotPsRo. Standard for pollution control of sewage marine disposal engineering; 2002. Available from: https://www.mee.gov.cn/ywgz/fgbz/bz/bzwb/shjbh/swrwpfbz/200201/t20020101_66558.shtml [Accessed 05-07 2025].
[54] N.L. Ukwattage, P.G. Ranjith, M.S.A. Perera, Effect of accelerated carbonation on the chemical properties and leaching behaviour of Australian coal fly ash, to improve its use as a compost amendment, Environ. Earth Sci. 75 (21) (2016) 1398, https://doi.org/10.1007/s12665-016-6188-y.
[55] Q. Yuan, Y. Zhang, T. Wang, J. Wang, Characterization of heavy metals in fly ash stabilized by carbonation with supercritical CO2 coupling mechanical force, J. CO_2 Util. 67 (2023) 102308, https://doi.org/10.1016/j.jcou.2022.102308.